Characterization of Porous Glasses: Simulation Models, Adsorption Isotherms, and the Brunauer−Emmett−Teller Analysis Method

Lev D. Gelb*,† and K. E. Gubbins†

School of Chemical Engineering, Olin Hall, Cornell University, Ithaca, New York 14853-5201

Received September 15, 1997. In Final Form: December 10, 1997

We have developed a realistic model for studying adsorption in porous glasses which reproduces the complex structure of these materials. The model porous material is generated by a quench molecular dynamics procedure which mimics the processes by which Vycor glass and controlled-pore glasses are produced. We examine this procedure and the resulting model materials by a variety of methods and find that they have porosities, pore sizes, and surface areas very similar to the real glasses. These simulated glasses have precisely known properties (surface area, pore size distribution, etc.), in contrast to experimental glasses; computer experiments on such model glasses can therefore be used to test new and existing experimental methods of characterization. We calculate the adsorption isotherms for a model of nitrogen adsorbing onto these materials and analyze these data using the BET isotherm. The BET monolayer density exhibits systematic variations with both the average pore size and the porosity of the model glasses, which can be partially explained by studying the variations of adsorption energies in the different systems. We have done similar calculations in a series of ideal planar and cylindrical pore systems with comparable surface micro-structure. We find that there is a systematic error involved in comparing the networked glasses to the ideal cylinders as is commonly done in the analysis of these materials. For glasses with large pores this error is negligible, but for very small pores it can be significant. We discuss the implications of these findings for other standard techniques of isotherm analysis.

1. Introduction

Controlled-pore glass is widely used as a stationary phase in chromatography.[1,2] Controlled-pore glasses (CPGs) and the related Vycor glasses have excellent mechanical properties and can be prepared with a wide range of porosities and average pore sizes.[3] They can be modified to include a variety of functional groups, and the adsorption strength of the glasses can be adjusted over a wide range of values.[1] Although controlled-pore glasses were developed for use in size-exclusion chromatography, derivatized glasses can show a high chemical affinity for certain biomolecules and can even be used as catalytic agents and bioreactors.[2]

Vycor glass is prepared[3] from a quaternary glass mixture, of typical composition 62.7% SiO_2, 26.9% B_2O_3, 6.6% Na_2O, and 3.5% Al_2O_3. This glass is melted and formed into the desired shape and then held at a temperature above the annealing point but below that which would cause deformation. The material phase-separates (on a microscopic scale) into two continuous phases, one rich in silica and the other in borosilicate and alkali. It is then treated with a hot dilute acid solution, which dissolves away the borosilicate phase. Lastly, Vycor is slowly heated to above 1200 °C. The finished glass is 96% SiO_2.

Vycors have a porosity near 28%, an average internal pore diameter somewhere between 4 and 6 nm, and a surface area of between around 90 and 200 m^2/g, calculated from BET analysis of nitrogen adsorption isotherms.[3]

The original preparations and characterizations of controlled-pore glasses were done by Haller.[4,5] CPGs are prepared like Vycor glasses. The starting material is 50−75% SiO_2, 1−10% Na_2O, and the remainder B_2O_3. The molten glass is phase separated by cooling to between 500 and 750 °C. The *time* taken for this treatment determines the extent of phase separation and the resulting average pore size. The borate phase is leached out by acid solutions at high temperatures. The remaining glass contains colloidal silica particles, which are removed by a treatment with NaOH followed by washing with water. The final glass has a porosity between 50% and 75%, and an average pore size between 4.5 nm and 400 nm. CPG has a surface area somewhere between 10 and 350 m^2/g, depending on the pore size.[1] An electron micrograph of a sample of controlled-pore glass with 300 nm pores is shown in Figure 1.

The porosity and surface area of porous glasses is usually determined using standard nitrogen adsorption techniques. Mercury intrusion porosimetry is also frequently used to estimate the pore size distribution of these glasses.[4] Although there has been considerable interest in the physics of flow, diffusion, and adsorption in these materials, there have been relatively few complete characterizations of porous glasses, and much of their structure is not very well understood.

Levitz et al.[6] characterized samples of Vycor glass using transmission electron microscopy, X-ray scattering, adsorption, and direct energy transfer. This study of the glass concluded that the Vycor structure is homogeneous at length scales much above the average pore size. They also found a surface roughness at length scales below 2 nm, where the local molecular structure of the material

† Present address: North Carolina State University, Department of Chemical Engineering, 113 Riddick Laboratories, Raleigh, NC 27695-7905.

(1) Schnabel, R.; Langer, P. *J. Chromatogr.* **1991**, *544*, 137.
(2) Haller, W. In *Solid Phase Biochemistry*; Scouten, W. H., Ed.; John Wiley and Sons: New York, 1983; p 535.
(3) Elmer, T. H. in *ASM Engineered Materials Handbook*; Schnieder, S. J., Jr., Ed.; ASM: Materials Park, OH, 1991; Vol. 4, p 427.
(4) Haller, W. *Nature* **1965**, *206*, 693.
(5) Haller, W. *J. Chem. Phys.* **1965**, *42*, 686.
(6) Levitz, P.; Ehret, G.; Sinha, S. K.; Drake, J. M. *J. Chem. Phys.* **1991**, *95*, 6151.

S0743-7463(97)01037-8 CCC: $15.00
Published on Web 03/20/1998

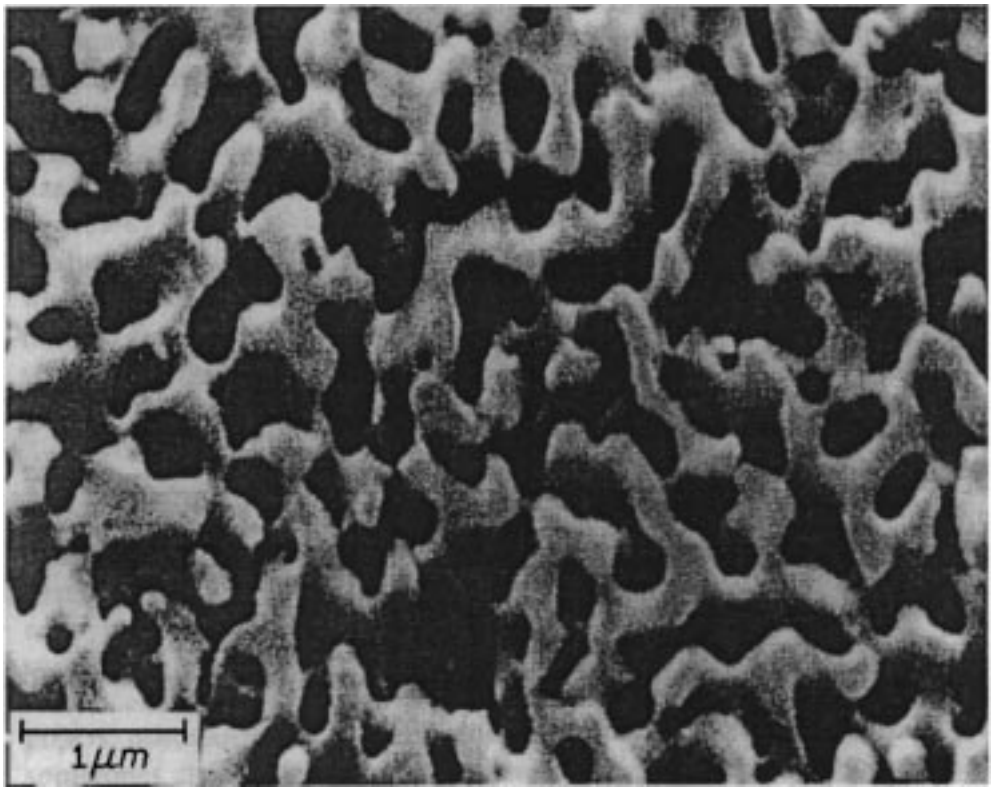

Figure 1. Scanning electron micrograph of controlled-pore glass of 300 nm mean pore diameter. Reprinted with permission from ref 2. Copyright 1983 John Wiley and Sons.

should be visible. The glass was found to have an average pore diameter of 7 nm from nitrogen desorption isotherm analysis. An earlier electron microscopy study of these glasses[7] compares a variety of direct measurement techniques for the average pore size, indicating that the average pore size of the material can vary by as much as 30% with different measurement techniques. The definitive model-based analysis of the structure of Vycor glass from adsorption isotherms is that of Mason,[8] who extracts cavity size distributions, the number of connections per cavity, the Kelvin pore size distribution, and the geometric pore size distribution.

The underlying process in the preparation of porous glasses is known as *spinodal decomposition*.[9,10] For mixtures where one component is dilute (at a concentration much less than the critical mole fraction), phase separation after a quench is by a droplet-condensation mechanism. When the two components occupy similar volume fractions, this mechanism changes to one that favors a locally tubular geometry. This decomposition process goes faster at late times and results in two completely connected phases with a complex-networked tubular geometry, with the average tube radius growing linearly with time.[9,11] This process is apparently universal, and the structure of the fluid at some time after the quench is determined by the viscosities of the two phases, surface tension, and starting mole fraction. A number of studies have shown that this growth is described well by a simple *scaling function*[11,12] and that many of the properties of the phase-separating systems are determined by a single length scale.

Adsorption in porous glasses is a complex phenomenon due to the networked structure and polydisperse pore size of the materials. Because the surface chemistry of controlled-pore glasses can be easily modified and the pore size distribution is relatively narrow (in comparison with many other adsorbents), these materials have often been used as substrates in studies of both liquid-liquid[13,14] and liquid−vapor[15−17] phase equilibria in confined systems.

For the most part, computer simulations of adsorption and liquid−liquid equilibria in Vycor glasses (and related materials) have focused on "single-pore models" where the adsorption of a gas into a small cylindrical or planar pore was studied in detail.[13,14,18−23] This scheme excludes effects due to the complex, highly networked geometry of porous glasses. These methods have been extended to include realistic atomic potentials for a number of adsorbates.[24−26] There are two serious difficulties in extending the standard simulation approach to study fully networked systems. The first is that it requires very large

(7) Enüstün, B. V.; Enuysal, M. *METU J. Pure. Appl. Sci.* **1970**, *3*, 82.
(8) Mason, G. *Proc. R. Soc. London, Ser. A* **1988**, *415*, 453.
(9) Siggia, E. D. *Phys. Rev. A* **1979**, *20*, 595.
(10) Chakrabarti, A. *Phys. Rev. Lett.* **1992**, *69*, 1548.
(11) Laradji, M.; Toxvaerd, S.; Mouritsen, O. G. *Phys. Rev. Lett.* **1996**, *77*, 2253.
(12) Ma, W.-J.; Maritan, A.; Banavar, J. R.; Koplik, J. *Phys. Rev. A* **1992**, *45*, R5347.
(13) Sliwinska-Bartkowiak, M.; Sikorski, R.; Sowers, S. L.; Gelb, L. D.; Gubbins, K. E. *Fluid Phase Equilib.*, in press.
(14) Sliwinska-Bartkowiak, M.; Sowers, S. L.; Gubbins, K. E. *Langmuir* **1996**, *13*, 1182.
(15) Thommes, M.; Findenegg, G. H. *Langmuir* **1994**, *10*, 4270.
(16) Thommes, M.; Findenegg, G. H.; Schoen, M. *Langmuir* **1995**, *11*, 2137.
(17) Findenegg, G. H.; Gross, S.; Michalski, T. *Stud. Surf. Sci. Catal.* **1994**, *87*, 71.
(18) Gelb, L. D.; Gubbins, K. E. *Phys. Rev. E* **1997**, *55*, 1290R.
(19) Gelb, L. D.; Gubbins, K. E. *Phys. Rev. E* **1997**, *56*, 3185.
(20) Peterson, B. K.; Gubbins, K. E.; Heffelfinger, G. S.; Marini Bettolo Marconi, U.; van Swol, F. *J. Chem. Phys.* **1988**, *88*, 6487.
(21) Peterson, B. K.; Walton, J. P. R. B.; Gubbins, K. E. *J. Chem. Soc., Faraday Trans. 2* **1986**, *82*, 1789.
(22) Tan, Z.; van Swol, F.; Gubbins, K. E. *Mol. Phys.* **1987**, *62*, 1213.
(23) Peterson, B. K.; Gubbins, K. E. *Mol. Phys.* **1987**, *62*, 215.
(24) Brodka, A.; Zerda, T. W. *J. Chem. Phys.* **1991**, *85*, 3710.
(25) Brodka, A. *Mol. Phys.* **1994**, *83*, 803.
(26) Brodka, A.; Zerda, T. W. *J. Chem. Phys.* **1996**, *104*, 6319.

(for a computer simulation, anyway) systems; a realistic model of a small chunk of even the smallest-pore-networked glass might involve hundreds of thousands of atoms. The second difficulty is that generating an appropriate pore structure is not trivial. Since the experimental materials are amorphous, there are no X-ray structures to use as templates (as is done in simulation studies of adsorption on zeolites) and generating an acceptable pore structure becomes harder than studying it!

The particular case of silica gels has been studied in some detail. A number of studies[27−30] have considered the gel matrix as a random collection of spherical silica "grains" and measured liquid−vapor equilibria,[29,30] diffusion,[27] and the structure of an adsorbed fluid at very low pressures.[28] The structural properties of collections of spheres have also been studied in depth,[31,32] although these properties have not been used to interpret adsorption data.

On a computer we can mimic the preparation of the real glasses by preparing a system that exhibits this kind of phase separation, quenching it, removing one phase, and relaxing or annealing the resulting structure. This procedure "naturally" produces a structure with the same general characteristics as the experimental glasses. By varying the length of the quench period and the starting mole fraction of the mixture, we can tune the surface area, porosity, and average pore size over a wide range of values.

This idea has been used several times in generating models for studies of phase separation and wetting in confined systems. MacFarland et al.[33] have studied the phase behavior of the Ising model confined in a porous medium. In this study of critical shifts and exponents, the porous material itself was made by a quench procedure in which an Ising system was allowed to partially relax by spinodal decomposition. The pore structure was characterized by measuring the large-k part of the structure factor. A similar procedure was used in a study by Strickland et al.[34] of the phase-separation kinetics of a two-dimensional binary mixture confined in a porous material. This approach has also been used in studies based on numerical solution of the Lattice−Boltzmann[35] and Cahn−Hilliard[10] models.

There are no empirical potentials available for the silicate−borosilicate system that show this phase separation, which is apparently due to anomalous bonding effects in the borosilicate.[36] The necessary size of the simulations (over one hundred thousand particles, for (at least) tens of picoseconds) precludes any attempt at *ab initio* simulation. So, we use a much simpler phase-separating system to generate the pore structure and then adjust the potentials to represent porous silica.

In this work we do two things. First, we present a method for simulating the formation of porous glasses that mimics the manufacture of real glasses. Since these simulated glasses are precisely characterized (we know the coordinates of every atom in the material), they can be used to simulate adsorption measurements and thus to test existing or proposed methods for characterizing porous glasses. Such tests are unambiguous, in contrast to experimental studies. The model glasses can also be used to investigate confinement effects such as selective adsorption from mixtures, phase changes, heats of adsorption, etc. The second part of our work consists of simulations of nitrogen adsorption in the networked glasses, and the use of these to evaluate the accuracy of the BET method for surface area determination.

For this study, we have prepared a series of model porous glasses with varying average pore size and porosity. The glasses all have very similar local surface structure, so that these systems can be used to study the differences in adsorption properties that result from changing the network structure and pore size in the glasses. We have also done similar calculations on a series of "ideal" systems of cylindrical, rodlike, and planar geometry, in order to compare networked with nonnetworked systems.

We have characterized these materials by a variety of geometric measures. We discuss a number of possible characterization tools that can be used in simulations and their relation to experimentally inferred effective quantities.

We have analyzed adsorption data in these systems using the Brunauer−Emmett−Teller (BET) isotherm,[37] which is frequently used to characterize real porous glasses. Although more sophisticated analysis techniques have been developed for adsorption data, the BET method remains a staple of materials characterization, and information about its accuracy (or inaccuracy) will be quite useful.

We have found that, for materials with pores smaller than about 4 nm diameter, use of the BET method of adsorption analysis leads to systematically high estimates of the surface area of the system, because the monolayer density in these systems is a function of pore diameter and increases for smaller pores due to the curvature of the surfaces. Furthermore, the porous systems and ideal cylinder systems exhibit qualitatively different behavior (of the monolayer density) for small pore systems. This may lead to a significant bias in using standard inversion techniques to obtain effective pore size distributions or surface energy distributions by modeling the glass as a collection of separate cylindrical pores. These differences appear to be due largely to the networked structure of CPG and the presence of both convex and concave sections of surface in the glasses. These effects are very small for systems with relatively large pores; since the range of diameter in porous glasses extends from around 4.5 to around 400 nm, these results are only applicable to the very low end of this class of materials. For glasses with larger pores it appears that the standard analysis methods should work well, as the surface curvature in these systems is too small to have any noticeable effect on the monolayer structure.

2. Preparation of Model Glasses

The model we use for the binary mixture in the quench calculations is a symmetrical Lennard-Jones fluid, a mixture of spherical particles of identical size with intermolecular potentials given by

$$U_{ij}(r) = \begin{cases} 4\epsilon_{ij}\left[\left(\frac{\sigma_{ij}}{r}\right)^{12} - \left(\frac{\sigma_{ij}}{r}\right)^{6}\right] - U_{ij}(r_c) & r \le r_c \\ 0 & r > r_c \end{cases} \quad (1)$$

(27) MacElroy, J. M. D.; Raghavan, K. *J. Chem. Phys.* **1990**, *93*, 2068.
(28) MacElroy, J. M. D. *Langmuir* **1993**, *9*, 2682.
(29) Page, K. S.; Monson, P. A. *Phys. Rev. E* **1996**, *54*, R29.
(30) Kaminsky, R. D. *J. Chem. Phys.* **1991**, *95*, 2936.
(31) Seaton, N. A.; Glandt, E. D. *J. Chem. Phys.* **1986**, *85*, 5262.
(32) Lu, B.; Torquato, S. *J. Chem. Phys.* **1993**, *98*, 6472.
(33) MacFarland, T.; Barkema, G. T.; Marko, J. F. *Phys. Rev. B* **1996**, *53*, 148.
(34) Strickland, B.; Leptoukh, G.; Roland, C. *J. Phys. A: Math. Gen.* **1995**, *28*, L403.
(35) Grunau, D. W.; Lookman, T.; Chen, S. Y.; Lapedes, A. S. *Phys. Rev. Lett.* **1993**, *71*, 4198.
(36) Skatulla, W.; Vogel, W.; Wessel, H. *Silikat. Technol.* **1958**, *9*, 51.
(37) Brunauer, S.; Emmett, P. H.; Teller, E. *J. Am. Chem. Soc.* **1938**, *60*, 309.

where $U_{ij}(r)$ is the potential between two particles of species i and j separated by a distance r. The properties of the mixture are determined by the ϵ_{ij} and σ_{ij} parameters. The mixture that we have studied is symmetric, with $\sigma_{11} = \sigma_{22} = \sigma_{12} = \sigma$, and $\epsilon_{11} = \epsilon_{22} = \epsilon$. To induce liquid−liquid phase separation, we weaken the unlike-pair attractive well-depth by setting $\epsilon_{12} = 0.25\epsilon_{11}$. r_c is a short-range cutoff used to greatly reduce the total cost of the simulations; in this study we have set it at 3.5σ (9.45 Å; see below). We have examined the properties of a similar mixture in previous work.[18]

Simulations of systems described by Lennard-Jones potentials are conveniently described in "reduced" units, where the fundamental unit of length is σ, the Lennard-Jones particle diameter, and the fundamental unit of energy is ϵ, the Lennard-Jones well-depth. Other quantities such as time and pressure have units which are functions of ϵ, σ, and the mass m.[38] In the results that follow we will quote experimentally comparable numbers (such as monolayer capacity and surface area) in standard units but will use reduced units for quantities which are internal to the simulation, such as the time step of the dynamics simulations and the parameters of the quench mixture.

Although this mixture is by no means a realistic model of the silicate/borosilicate system, the phase separation process is not dependent on the details of the mixture and the pores formed by using these liquids should be of the same general shape and type as the pores in real glasses. It appears that the process of phase separation under near-critical quenching is universal (at least, widely different systems all show very similar properties and structures), so it is not necessary to use a sophisticated model for the quench mixture if all we require is a structure with similar networking properties.

The phase separations are done using quench molecular dynamics (Quench-MD)[18] at constant density. In a molecular dynamics calculation, the classical equations of motion for the system are integrated forward in time using a finite-difference algorithm. Refinements to this method allow for constant temperature simulations to be performed using modified equations of motion.[38] In the Quench-MD method, the system is equilibrated at a high temperature until the energy and liquid structure have stabilized. After that, the thermostat is reset to a lower temperature and the system relaxes toward equilibrium at the new temperature. In the case of a phase-separating binary mixture, this relaxation may be slow.[18]

The number of particles in a computer simulation study typically ranges from a few hundred to a few thousand. These small system sizes are augmented by "periodic boundary conditions" in the simulation cell, which attempt to describe a (macroscopic) real system by an infinite lattice of identical cells, each with a relatively small number of particles. In our calculations, the minimum size of the cell is determined by the average pore size we wish to generate. The periodic structure imposed by the boundary conditions can interfere with the phase separation process at late times (large domains) and favor unnatural domain structures. We have found that for the pore structure to be not strongly affected by the periodic simulation cell, the side of the box must be at least three times larger than the desired pore diameter. In order to create a glass with 6 nm diameter pores, the largest used in this study, we have used a simulation cell approximately 16 nm on each side. The average pore diameter of the model glass is determined by the length of time the system is quenched, and the porosity of the glass is a function of the quench time and the initial mole fraction.

These calculations were done on the IBM SP2 computer at the Cornell Theory Center, typically using 28 processors. The quench runs for the systems studied in this paper took approximately three thousand processor-hours of computer time. The simulation program is based on a three-dimensional domain decomposition scheme in which each processor handles a fixed volume of the system.

Finally, to study the adsorption of nitrogen on silica, we model the nitrogen molecules by a single Lennard-Jones sphere, setting its parameters $\sigma_N = 0.375$ nm and $\epsilon_N/k_B = 95.2$ K.[39] The Lennard-Jones parameters for the substrate atoms are set to $\sigma = 0.27$ nm and $\epsilon/k_B = 230$ K, which have been used to represent bridging oxygens in silica.[24] Following previous simulations of adsorption on silica gels, we omit the silicon atoms from the calculation; their small size and low polarizability make this an acceptable approximation.[28,24] The parameters controlling the interaction between the nitrogen molecules and the pore atoms are $\sigma_{N-P} = 0.322$ nm and $\epsilon_{N-P}/k_B = 147.9$ K, in accord with the Lorentz−Berthelot mixing rules. The density of the fluid throughout the quenching process is (in reduced units) $0.868\sigma^{-3}$, which reproduces the density of the oxygen atoms in a silica glass of density 2.2 g/cm^3.

The complete preparation recipe for the model glasses used in this study is as follows:

1. A system of 175 000 particles in a simulation cell measuring 58.64σ on each side, with a mole fraction of species "1" between 0.5 and 0.7 is prepared as a crystal, melted, and equilibrated at $k_BT = 5.00\epsilon$ for 4000 time steps of length 0.005τ. A Gaussian isokinetic thermostat and third-order Gear predictor−corrector integrator are used throughout.

2. The system is quenched to $k_BT = 0.75\epsilon$ in a single step and run for between 7500 and 90 000 more time steps, depending on the desired pore size.

3. The final configuration from the quench run is quenched further to $k_BT = 0.01\epsilon$ for an additional 1000 time steps to relax the surface structure and solidify the material.

4. The "2"-rich phase is removed from the system. Uncoordinated molecules of component "1" are also removed.

A series of snapshots from a quench run at $X = 0.6$ are shown in Figure 2. At zero time, the two liquids are well mixed. At later times the liquids separate in a complex way, forming *fully connected* networked structures which resemble cylinders at a very local scale but have many "defects" and intersections. As time progresses this structure grows slowly but does not seem to change much in character.

Domain size and energy relaxation data from this quench run are shown in Figure 3. As the quench progresses, the average domain size (see below) grows according to a power law with exponent near 0.5, and the excess potential energy of the system decreases by a power law with exponent near −0.5. (The excess potential energy is a measure of the total interfacial area in the system, which is inversely proportional to the average domain size.) By stopping the quench at a particular time, the average pore size can be specified in advance. It may be possible to predict the degree of networking from the fluid mechanical properties of the two components of the mixture; we have not yet attempted this as it would require

(38) Allen, M. P.; Tildesley, D. J. *Computer Simulation of Liquids* Clarendon Press: Oxford, 1987.

(39) Maddox, M. W.; Olivier, J. P.; Gubbins, K. E. *Langmuir* **1997**, *13*, 1737.

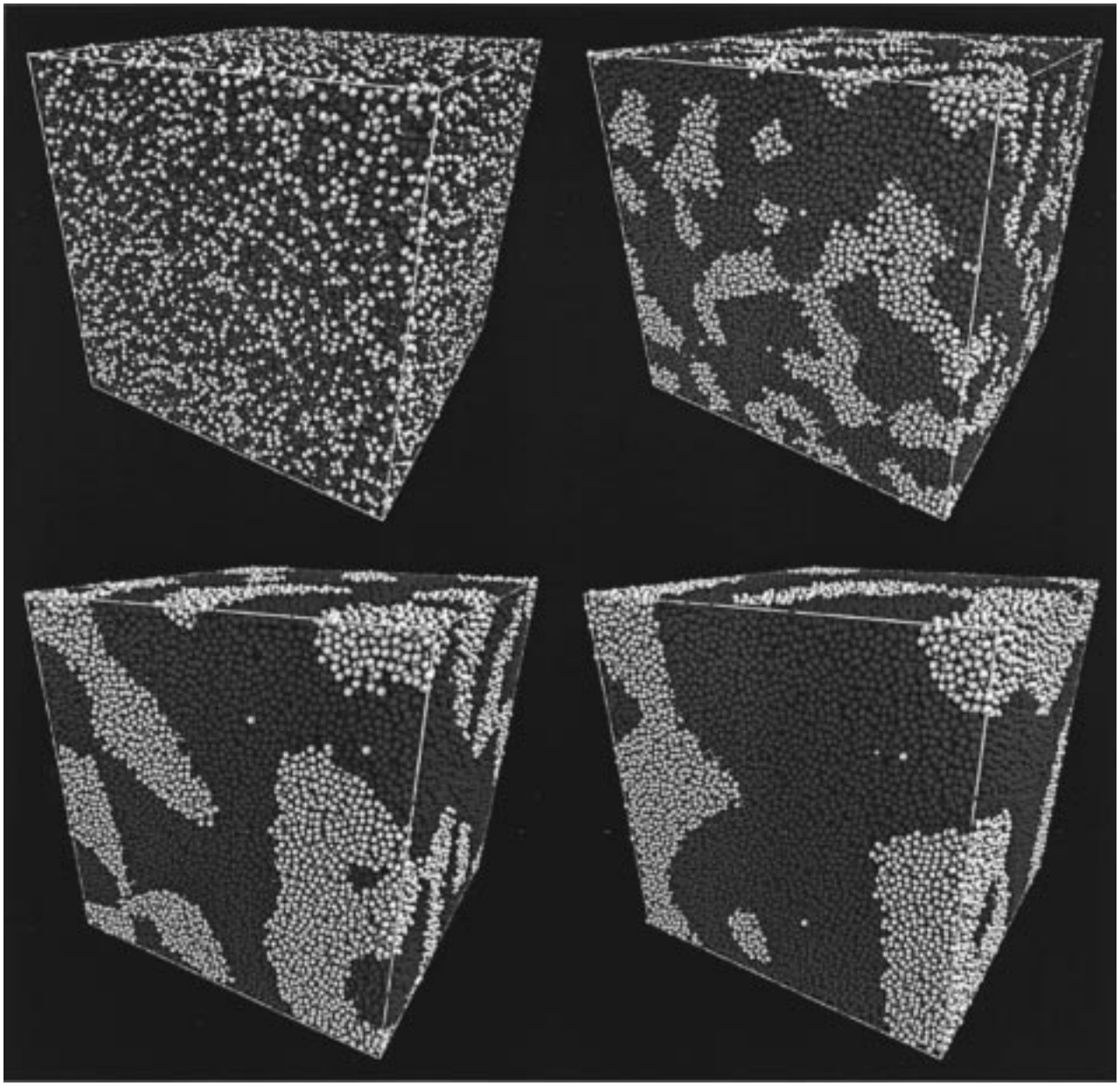

Figure 2. Snapshots of the quench run at mole fraction $X = 0.6$. The upper left configuration is taken at $t = 0\tau$ (reduced time units), the upper right configuration at $t = 75\tau$ (used to make the (6a) CPG system), the lower left configuration at $t = 225\tau$ (the (6c) CPG system), and the lower right configuration at $t = 450\tau$ (the (6d) CPG system). See the text for the procedure used to name the different CPG systems.

a considerably larger number of quench simulations and reliable measures of the topological connectivity of the glass.

2.1. Model Systems. We have prepared three different series of model glass systems, starting with three different initial mole fractions of $X = 0.5$, $X = 0.6$, and $X = 0.7$, resulting in systems with porosities around 50%, 40%, and 30%, respectively. For each system, we have run the quench simulation for 90 000 time steps and taken the configurations after 15 000, 30 000, 45 000, and 90 000 time steps (75, 150, 225, and 450 reduced time units (τ), respectively) for use as model pore systems. CPG models from quenches at 15 000 time steps are group "a", models made from configurations at 30 000 time steps are group "b", etc. In our labeling system, the (7c) model is a structure taken from a quench at a mole fraction of 0.7, after 45 000 time steps, while (5d) is a structure taken from a quench at $X = 0.5$ after 90 000 time steps. Characteristics of each of these 12 pore systems are shown in Table 1.

We have also prepared a series of pores of "ideal geometry" for comparison with the model glasses. For these systems we equilibrated a system of a single component of the quench mixture at $k_B T = 0.75\epsilon$, removed some of the material to form a cylindrical, rod-shaped, or planar pore, and then relaxed the system at $k_B T = 0.01\epsilon$ for 1000 time steps. This procedure produces surfaces with the same local atomic structure as our model porous glasses, but with easily controlled geometries. The ideal systems are made in a simulation cell 38.62σ on each side that initially contains 50 000 particles, for the same density as the quench systems. We have made five cylindrical pores of different diameters, five rodlike adsorbents of different diameters, and a single planar-

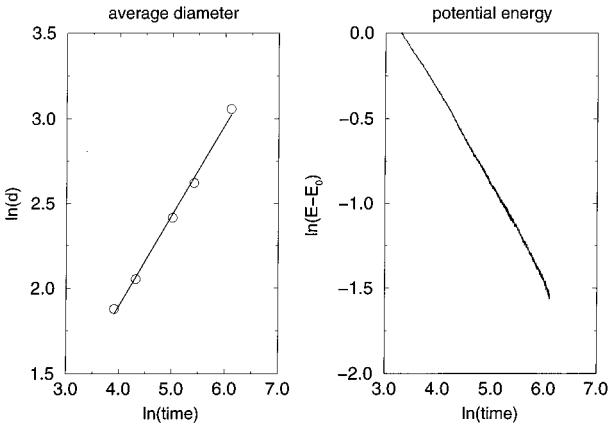

Figure 3. Relaxation data for the quench run at mole fraction $X = 0.6$. The graph on the left shows the average domain size (units of σ) as a function of reduced time, on a log−log plot. The straight line indicates a power-law dependence. The graph on the right shows the energy per particle relative to the fully relaxed state ($E - E_0$), which also shows a power-law dependence. The slope of the domain data is ≃0.5, and the slope of the energy data is ≃−0.5.

Table 1. Properties of the Porous Glass Systems[a]

system	$\bar{d}$ (nm)	porosity	surface area (m^2/g)	ρ_m (nm^{-2})	$\bar{U}_{surf}$ (kJ/mol)
(5a)	2.12(7)	0.3894(11)	264.1(13)	5.24(16)	−4.63
(5b)	3.00(7)	0.4360(12)	178.3(7)	4.65(8)	−4.55
(5c)	3.82(7)	0.4640(13)	131.4(9)	4.47(5)	−4.53
(5d)	5.45(7)	0.4877(14)	93.9(8)	4.43(5)	−4.51
(6a)	2.11(7)	0.3037(9)	277.7(13)	5.46(11)	−4.93
(6b)	3.02(7)	0.3502(10)	190.8(12)	4.83(10)	−4.74
(6c)	3.71(7)	0.3723(11)	152.8(10)	4.61(7)	−4.67
(6d)	5.74(7)	0.4001(11)	96.9(9)	4.42(7)	−4.63
(7a)	2.03(7)	0.2203(6)	271.3(15)	5.38(8)	−5.43
(7b)	2.92(7)	0.2636(7)	192.2(11)	5.06(11)	−5.07
(7c)	3.81(7)	0.2869(8)	152.7(10)	4.75(10)	−4.88
(7d)	6.08(7)	0.3093(9)	98.6(7)	4.49(5)	−4.72

[a] $\bar{d}$ is the average pore diameter measured from the radial distribution function in the quench system. The porosity is a fractional measure and does not have units. ρ_m is the BET *monolayer density*. $\bar{U}_{surf}$ is the average of the geometrically measured surface energy distribution. Uncertainties in the last significant figure are quoted in parentheses.

surface system. (We have made rod-shaped adsorbents to examine the effects of convex curvature on the monolayer properties.) In previous work we have used smooth cylindrical[40] and planar[41] pore systems; in this study we use models of the ideal geometries having structured, molecular surfaces for better comparison with the model porous glass systems. The geometric properties of these systems are shown in Table 2.

3. Geometrical Analysis of Model Glasses

We determine the geometric properties of the glass using Monte Carlo methods related to those developed for stereological studies.[42] In these calculations we have three-dimensional descriptions of the pore systems, so that the two-dimensional methods of traditional stereological analysis need to be modified to take advantage of this additional information.

3.1. Definitions of Molecular Surface. There are a number of ways of defining a molecular surface, which

(40) Gelb, L. D.; Gubbins, K. E. *Physica A* **1997**, *244*, 112.
(41) Suzuki, T.; Kaneko, K.; Setoyama, N.; Maddox, M.; Gubbins, K. *Carbon* **1996**, *34*, 909.
(42) Underwood, E. E. *Quantitative Stereology;* Addison-Wesley: Reading, MA, 1970.

Table 2. Properties of the Ideal Geometry Systems[a]

system	"d"	ρ_m (nm^{-2})	$\bar{U}_{surf}$ (kJ/mol)
5σ rod	2.70	4.18(7)	−4.07
7σ rod	3.78	4.23(7)	−4.25
9σ rod	4.86	4.25(7)	−4.34
12σ rod	6.48	4.27(7)	−4.42
15σ rod	8.10	4.32(7)	−4.46
plane	∞	4.36(5)	−4.63
5σ cylinder	2.70	4.97(7)	−4.99
7σ cylinder	3.78	4.77(7)	−4.88
9σ cylinder	4.86	4.64(7)	−4.84
12σ cylinder	6.48	4.50(5)	−4.78
15σ cylinder	8.10	4.50(5)	−4.76

[a] "d" is the approximate diameter of the pore. ρ_m is the BET *monolayer density*. $\bar{U}_{surf}$ is the average of the geometrically measured surface energy distribution. Uncertainties in the last significant figure are quoted in parentheses.

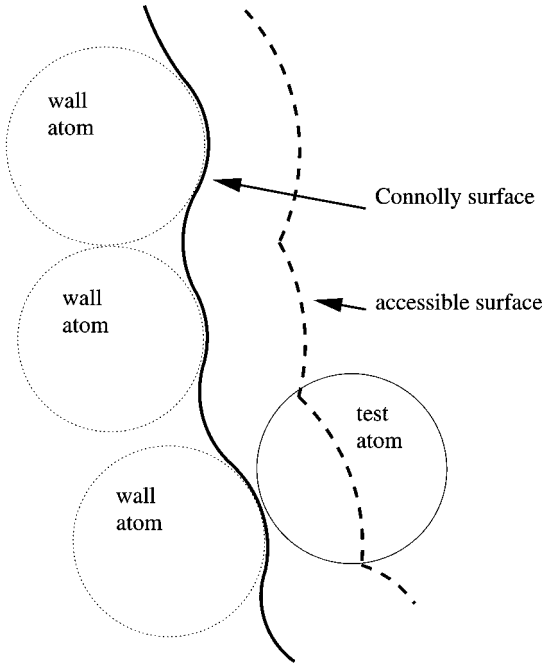

Figure 4. Two-dimensional representation of the different definitions for a molecular surface. As a test atom is moved across the pore surface (wall atoms), its *edge* traces the Connolly surface (solid line), while its *center* traces the accessible surface (dashed line). Both surfaces are corrugated on a molecular scale.

all yield different pore volumes, surface areas, etc. For very large pores, different definitions of the molecular surface give similar results because the differences are always of the order of one molecular diameter. For microporous and mesoporous materials these different definitions can give significantly different results and can have different qualitative behavior as well.

There are two common definitions of molecular surface. A schematic drawing of these surfaces is shown in Figure 4. The outer (dashed) line is the "accessible surface", which is the locus of points of the *center* of a probe molecule in contact (defined as $1\sigma_{N-P}$ distance) with one or more pore atoms. This definition of the pore surface (and accompanying volume) is useful in statistical mechanical calculations, since it is this volume that essentially determines the entropy of a confined ideal gas. However, use of the accessible surface leads to some unpleasant behavior of the density in narrow pores. For instance, in a planar pore of width 3σ (measured between the centers of atoms in the two walls), two full monolayers can form, but the "accessible" part of the width is only 1σ, which leads to a "full pore" density around $2\sigma^{-3}$, twice the density

of the bulk solid! This problem is often corrected for by adding $\sigma/2$ to each side of the pore, to represent the volume accessible to all parts of the adsorbed molecules.[18,41,43] This correction cannot be made in pores of complex geometry.

This leads to a second definition of a molecular surface, which is often called the "reentrant surface" or "Connolly surface".[44,45] This is the surface traced by the *outside* of a test particle "rolled" over the pore wall (solid line, Figure 4). Put another way, the volume defined by this surface is the volume accessible to *any part* of a test molecule on (or outside of) the accessible surface. The Connolly volume (of a pore) is always larger than the accessible volume.

Connolly surfaces are used extensively in biomolecular calculations, as they are the "right" surface to use for measuring whether a molecule will fit inside the active site of an enzyme, for example. In the case of a porous system, if the pore is 2 nm wide, defined by a Connolly surface, then a molecule 2 nm wide (also defined by a Connolly surface) will almost certainly fit in it. That is, the Connolly surface has the desired "mechanical" properties for characterizing a material while the accessible surface has the desired thermodynamic properties.

For both of these molecular surface definitions, the results obtained depend on the size (and shape) of the probe molecule used to define the surface. For very large pores these differences are minimal, but for pores less than 10 or 20 nm across they can be significant. Since most of the common adsorbate "test" gases (such as nitrogen, argon, and methane) are of similar size, the properties calculated with them are similar, but in a 3 nm porous glass the accessible volume of a sulfur hexafluoride molecule will differ significantly from that of a nitrogen molecule. For all of the structural properties directly calculated in this paper, we have used our model of nitrogen as the test particle and the accessible surface definition.

Experimentally, average pore widths are often obtained by neutron diffraction. These widths do not correspond to either of these two definitions; since the neutrons measure the positions of the atomic nuclei in the pore walls, they find a surface which is *inaccessible* to *any* part of the adsorbed molecules.

We note that all of the networked systems that we have studied are *fully connected*, so that an adsorbed molecule can explore the entire network and there are no inaccessible open spaces. This can be verified either by looking at a succession of thin sections of the pore system or by filling it with adsorbate at high pressure and using a *cluster counting* algorithm to determine if all of the adsorbate is in a single cluster.[38] Nevertheless, we sometimes refer to multiple "pores" because the structure of the material can be logically subdivided into a collection of individual pores which meet at junctions.

3.2. Porosity. The porosity of the glass is just the volume fraction not taken up by the substrate. We determine this by Monte Carlo integration. Test points are placed randomly in the simulation box. If an adsorbate particle placed at a test point overlaps with the pore material (that is, is inside the accessible surface), the point is accumulated as a "hit," and the estimated porosity is just the number of misses divided by the total number of insertions. Porosities calculated in this way agree well with those obtained by helium adsorption at high temperatures[43] but are more easily calculated.

The porosities of the model glass systems are shown in Table 1. The porosity is a weak function of the quench time for all of these systems; as the pores become larger, the porosity approaches the initial mole fraction of component "2". For systems with small pores (short quench runs) the porosity is lower. This is because of the use of the accessible surface definition; for small pores, the space excluded by the wall atoms is a larger fraction of the total volume than it is for large pores. The porosity measured in this way slightly exceeds the initial mole fraction X_2 for the (6d) and (7d) glasses; this is due to contraction of the pore material as it is annealed at very low temperature.

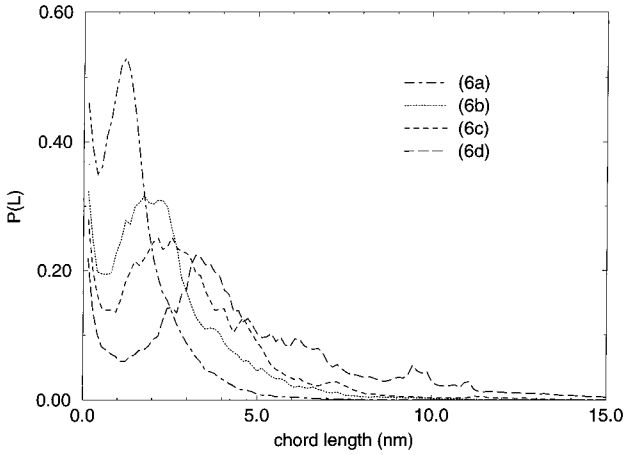

Figure 5. Chord length distributions for the "6" series of model CPG materials, from stereological analysis.

3.3. Surface Area. The surface area per unit volume can be determined in a similar fashion. Line segments are drawn randomly through the system, and the number of *intersections per unit length* is determined. This quantity is equal to half the surface area per unit volume.[42] In practice, we find intersections by dividing the lines into a grid and testing whether each grid point overlaps with the pore material. Accessible surface areas for all of the systems we have studied are shown in Tables 1 and 2. Note that the (7d) system has very nearly the same porosity, average pore size, and surface area as the Vycor sample studied by Levitz et al.[6] The Levitz study finds an average pore size of 7 nm (compare with our 6.08 nm), a porosity of 0.30 (compare with our 0.3093), and a surface area of 91 ± 5 m^2/g, quite close to our value of 98.6 ± 0.7 m^2/g.

3.4. Chord-Length Distribution. In the calculation of surface area, we accumulate a histogram of the lengths of lines between intersections. This is called the *chord-length distribution* and is related to the shape distribution of free volume in the system. For the particular case of a material composed of polydisperse, randomly placed spheres, this distribution can be exactly inverted to give the sphere size distribution. For more complex systems this inversion is not possible. However, the distribution itself seems to be characteristic of the pore structure, and can be used to compare different materials. Chord-length distributions have now been determined for samples of Vycor glass, from electron microscopy images.[6]

A series of these distributions is shown in Figure 5. Each distribution is composed of a peak at very short chord lengths and a broader, asymmetric peak at larger lengths. The peak at short chord lengths is due to the roughness of the surface at a molecular scale. The second peak is centered near or slightly below the average pore size (measured from the radial distribution function, see below) and its width may be characteristic of the width of the pore size distribution in the system. The tail at large

(43) Myers, A. L.; Calles, J. A.; Calleja, G. *Adsorption* **1997**, 3, 107.
(44) Connolly, M. L. *J. Appl. Crystallogr.* **1983**, *16*, 548.
(45) Connolly, M. L. *J. Am. Chem. Soc.* **1985**, *107*, 1118.

lengths indicates that the local structure of the pores is cylindrical; these are chords that pass axially through the pores, rather than across them. As the pore size increases, the quality of these data decreases due to a decreasing number of pore sections over which to average. There is some structure in the distribution for the (6d) system; this probably indicates that the system is not large enough to contain a representative quantity of the substrate; if there are not enough pores in the cell, these curves will visibly reflect the structure of individual pores.

3.5. Average Pore Size. One geometrical measure of the average pore size is found in the radial distribution function of the pore particles. This function has a long-wavelength component which is often taken as a measure of the average domain size in studies of spinodal decomposition of binary mixtures.[46,47] It does not contain information about the pore structure or degree of connectivity. This measure compares favorably with data from small-angle-scattering experiments, which measure long-wavelength fluctuations in concentration.[48,49] The average pore sizes determined in this way for our model glass systems are shown in Table 1. We have found that this measure agrees well with the average of the chord length distribution (see above).

3.6. Energy Distributions. Many porous materials, even ones that do *not* have active groups or chemical inhomogeneity, have a wide distribution of surface adsorption energy which can be used to describe the material in the same way that the pore size distribution can be used.[50] This is usually obtained by numerical inversion of adsorption data.[39,51] Such a distribution is an effective quantity that is basically defined by its calculation and is not necessarily a unique function of the adsorption data. In simulation studies we can calculate a number of related quantities directly from the pore structure.

3.6.1. Surface Energy Distributions. This is the distribution of potential energy of a test molecule placed within some small distance (0.3 Å, for results presented here) of the accessible pore surface. It reflects the environment seen by an adsorbed gas at low temperatures and pressures. The average over this distribution is a measure of the average potential energy of a molecule in contact with the surface, which is related to the absolute isosteric heat of adsorption. These values are arithmetic averages, rather than Boltzmann-weighted averages. They are shown for all systems in Tables 1 and 2.

A series of these distributions, for the "6" series of CPG model materials, is shown in Figure 6. These curves are all very similar, which reflects the similar molecular structure of the surfaces for these systems. As the pore size increases, the surface energy distribution more closely resembles that of the planar surface. For smaller pores, there is a noticeable "shoulder" on the low-energy part of the distribution curve, which contributes to the lower average surface energies for these systems (Table 1). Lastly, even the (6d) system distribution is not as sharp as the planar distribution, indicating significant curvature effects in this system.

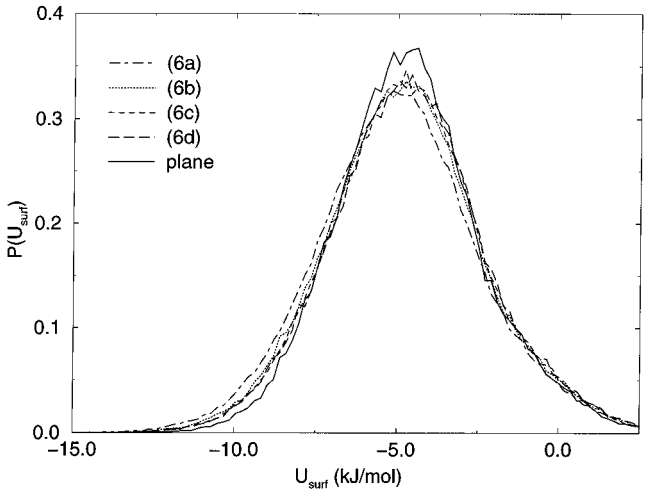

Figure 6. Surface energy distributions for the "6" series of CPG systems. The energy distribution for the planar surface is shown for comparison.

These curves are not directly comparable with surface energy distributions calculated from adsorption isotherm data.[51] In those procedures, an *effective* energy distribution is obtained by modeling the surface of the material as a collection of surfaces with different adsorption energies and fitting this collection so as to reproduce the experimental isotherm. In real glasses (and our models), the surface is homogeneous on a length scale much above 1 nm, so that most of the energetic heterogeneity is at a very small scale and areas with different adsorption energy cannot be separated. Furthermore, those procedures do not take into account the local curvature of the surface, which we will show has a significant effect on adsorption in small pores.

3.6.2. Volume Energy Distributions. This is the distribution of potential energy of a test molecule placed *anywhere* in the system. In statistical mechanical terms, it is the density of states of a lone adsorbed gas molecule. This is an enormously useful quantity. The low-coverage adsorption data can be calculated from it at any temperature by assuming that the adsorbate molecules do not interact with each other. This distribution not only reflects energy inhomogeneity at the surface but also contains information about the pore size distribution. Although this quantity has rarely been considered in the analysis of adsorption data, we believe that with very low-pressure adsorption data at several temperatures it may be possible to uniquely determine this function from experimental data and will attempt such an inversion of simulated adsorption data when it becomes available.

3.7. Surface Roughness. Both the Connolly and accessible surfaces are corrugated on a molecular scale, so that these surface areas will always be larger than those calculated from geometric assumptions about the system. For instance, in the case of a flat planar surface, we can calculate the "ideal" area of the plane by multiplying the lengths of its edges; for a spherical particle in a silica gel we could calculate its surface area from its radius. These areas are smaller than either the accessible or Connolly surface areas. For all of the ideal systems we have studied, we find that the ratio of "ideal" surface area to accessible surface area is very near to 1:1.20. For the model glasses, we cannot measure an "ideal" area. The local curvature of these surfaces is similar to that of the cylinders, so we expect that a similar roughness parameter might be applicable. In the results that follow, we do *not* apply any correction to account for this roughness. This

(46) Velasco, E.; Toxvaerd, S. *Phys. Rev. Lett.* **1993**, *71*, 388.
(47) Keblinski, P.; Ma, W.-J.; Maritan, A.; Koplik, J.; Banavar, J. R. *Phys. Rev. E* **1993**, *47*, R2265.
(48) Wiltzius, P.; Dierker, S. B.; Dennis, B. S. *Phys. Rev. Lett.* **1989**, *62*, 804.
(49) Lin, M. Y.; Sinha, S. K.; Drake, J. M.; Wu, X.-I.; Thiyagarajan, P.; Stanley, H. B. *Phys. Rev. Lett.* **1994**, *72*, 2207.
(50) Lastoskie, C.; Gubbins, K. E.; Quirke, N. *Langmuir* **1993**, *9*, 2693.
(51) Olivier, J. P. In *Fundamentals of Adsorption*; LeVan, M. D., Ed.; Kluwer Acad. Pub.: Boston, MA, 1996; p 699.

leads to relatively *low* estimates (compared with experiment) for the monolayer density in these systems.

4. Adsorption Isotherms

Grand Canonical Monte Carlo is a stochastic scheme which simulates an *open* system characterized by fixed temperature, chemical potential (or activity), and volume. It is the appropriate method to use for determining adsorption isotherms by computer simulation. The specific details and mathematics of this scheme can be found elsewhere.[38,52,53]

For the simulations in the model glass systems, each isotherm point was equilibrated for at least 20 million moves, followed by data collection for at least 10 million more moves. This resulted in average densities (loadings) accurate to within 1%. For the ideal pore systems each point was equilibrated for 6 million moves followed by 10 million moves of data collection, resulting in similar quality data. In most cases displacement, insertion, and deletion moves were performed with equal probability. (We found that the results were insensitive to the choice of move schedule.) Maximum particle displacements were adjusted to give a 50% acceptance ratio. The model glass simulations were run primarily on a 433 MHz Digital workstation; each point on each isotherm took approximately 5 h on this machine.

In order to convert absolute adsorption data (measured in the simulation as molecules per volume adsorbate vs chemical potential) to mmol/g vs relative pressure P/P^0, we have used the virial equation of state and the geometric porosity of the system.[43] The second virial coefficient can be exactly calculated from the molecular pair potential. We have also determined the saturation pressure P^0 for the adsorbate with Gibbs Ensemble Monte Carlo simulations.[54] We have not used published equation of state data for this fluid because of details of the potentials used. As stated above, we have used a "cut-and-shifted" Lennard-Jones potential *without* applying any sort of long-range correction. This is necessary because such a correction in the networked pore systems would be difficult to apply without bias but means that we cannot use published equation of state data for the fluid, since these data always contain corrections.[55]

We have low-pressure isotherm data for all of the systems described above and high-pressure isotherms showing capillary condensation (type IV) behavior[56] for several of the model glass materials.

Adsorption isotherms from all of the ideal systems that we have studied are shown in Figure 7. Since we are principally concerned with the estimation of surface areas in this study, we have not run these isotherms to high pressure. For these systems, while cylinders and rods of comparable diameter have similar surface areas, they have different substrate densities (that is, different numbers of wall atoms in the simulation cell), which causes a scaling of the adsorption isotherms when reported in units of mmol/g. As a result, the absolute scale of the isotherms for the rod systems is larger than that for the cylindrical systems. We note that as the curvature progresses from strongly convex (small rods) to zero (planar) to strongly concave (small cylinders) the shoulder of the adsorption isotherm become progressively sharper; this reflects the increasingly attractive potential energy at the surface.

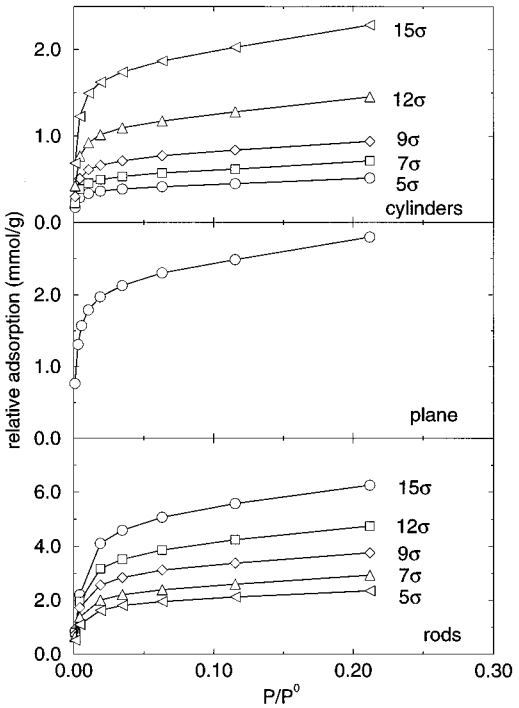

Figure 7. Adsorption isotherms (low-pressure data) for all of the ideal geometries we have studied; rods, cylinders, and a planar surface. Adsorption is given in units of millimoles of adsorbate per gram adsorbent.

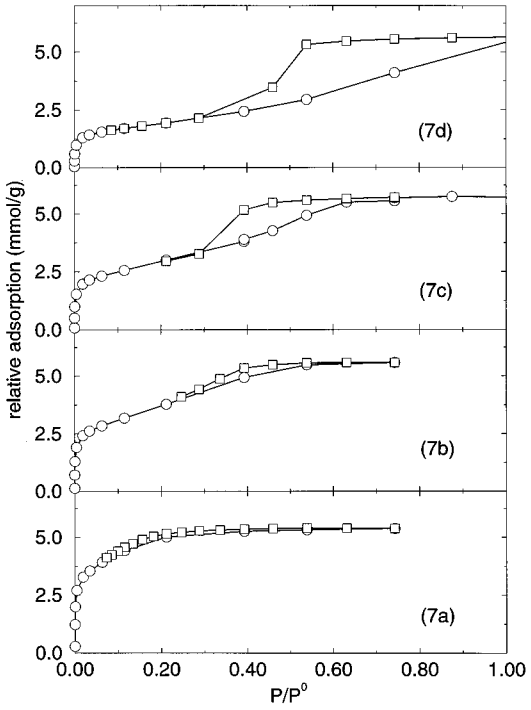

Figure 8. Adsorption and desorption isotherms in the "7" series of CPG model materials. Adsorption is given in units of millimoles of adsorbate per gram adsorbent.

Adsorption and desorption isotherms for the four different CPG models in the "7" series are shown in Figure 8. In the (7a) and (7b) systems, which have very small pores, capillary condensation is suppressed and the isotherms are nearly reversible. In the (7a) system, the isotherms appear to be type I, as typically seen in microporous solids. While this system does not quite fit

(52) Adams, D. J. *Mol. Phys.* **1975**, *29*, 307.
(53) Cracknell, R. F.; Nicholson, D.; Quirke, N. *Mol. Phys.* **1993**, *80*, 885.
(54) Panagiotopoulos, A. Z. *Mol. Phys.* **1987**, *62*, 701.
(55) Nicolas, J. J.; Gubbins, K. E.; Streett, W. B.; Tildesley, D. J. *Mol. Phys.* **1979**, *37*, 1429.
(56) Evans, R.; Marini Bettolo Marconi, U.; Tarazona, P. *J. Chem. Phys.* **1986**, *84*, 2376.

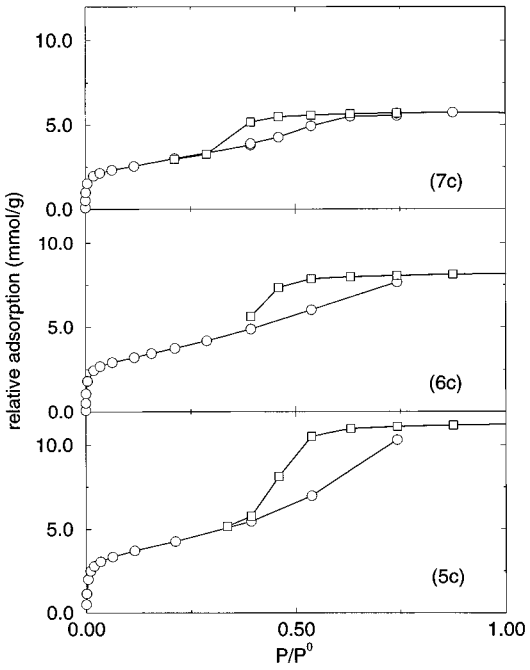

Figure 9. Adsorption and desorption isotherms for the three different CPG models with average pore size near 3.8 nm ("c" group.) The uncertainty in the data is smaller than the symbols used. Adsorption is given in units of millimoles of adsorbate per gram adsorbent.

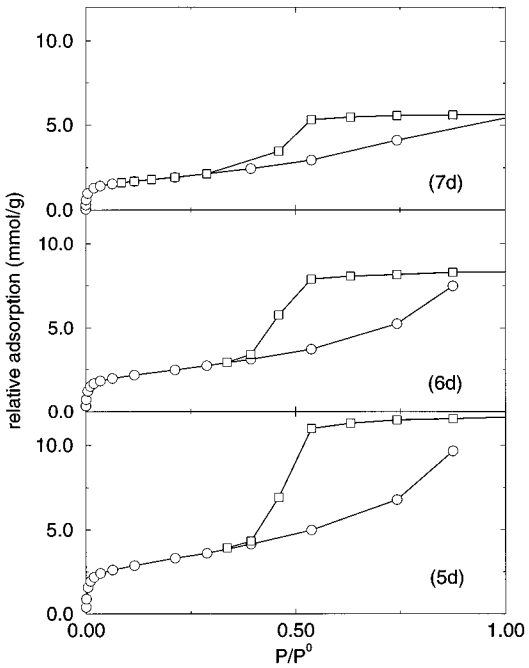

Figure 10. Adsorption and desorption isotherms for the three different CPG models with average pore size near 6.0 nm ("d" group.) The uncertainty in the data is smaller than the symbols used. Adsorption is given in units of millimoles of adsorbate per gram adsorbent.

the definition of a microporous solid,[57] it contains many pores which are well within the micropore range. In the two larger systems there is considerable hysteresis in the isotherm data, indicating the presence of a first-order capillary condensation transition. We note that in Monte Carlo simulations of adsorption, hysteresis is due to the presence of thermodynamically metastable states in the system and *not* to kinetic effects such as "pore-blocking".

In Figure 9 are isotherms for the three different CPG model materials (5c), (6c), and (7c), which all have average pore diameters near 3.8 nm (see Table 1) but have different average surface energies and porosities. As the porosity is increased, the hysteresis loop becomes more pronounced and moves to slightly higher pressures. This shift is typical in mesoporous materials; as the pore size is increased, the condensation pressure moves toward the saturation pressure.

Isotherms for the three systems in the "d" group (with average pore diameters near 6 nm) are shown in Figure 10. These systems all have very pronounced hysteresis loops, which occur at higher pressures than those in the "c" group (Figure 9), which have smaller pores. There does not appear to be any dependence of the position of this loop on the porosity of the sample. These isotherms are remarkably similar to published isotherms for krypton and xenon on Vycor glass, which has a similar average pore size.[58]

A series of four snapshots from the adsorption run in the (6c) CPG system is shown in Figure 11. At low pressures particles only adsorb on the most favorable sites. As the pressure is increased, a full monolayer gradually forms. In the third snapshot, at approximately the BET monolayer formation pressure, the monolayer is not of uniform thickness; on very concave parts of the surface ("hollows") it is thicker than on convex parts of the surface. Also, bridges form at constrictions of the pores, sometimes extending as far as eight molecular diameters. In the last snapshot capillary condensation has clearly occurred, and the pores are filled with liquid. From snapshots and total adsorption data (Figure 9) we see that the pores fill gradually and that there are not discrete "condensation points" in different parts of the network. (Discrete condensation behavior has been seen in a model of a repulsive-walled silica gel,[29] which displayed well-defined different condensation pressures in different sections of the network. The same study found that these effects were suppressed in attractive-walled gel models.[29]) In these snapshots particles are color-coded according to their potential energy, which shows that the different adsorbed layers have different energetic properties.

A series of snapshots from the adsorption run in the (6d) system is shown in Figure 12. In this system the pores are larger and the local curvature is generally smaller than in the (6c) material, so that no bridges are visible at monolayer filling, and the monolayer appears to be more uniform. Also, in the last snapshot capillary condensation has not yet occurred, although the adsorbed layer seems to be three or four monolayers thick and bridges have formed across constrictions in some places. The adsorption data (Figure 10) show that this system, like the (6c) system, fills smoothly, without any steps in the isotherm.

5. BET Analysis of Adsorption Data

The Brunauer−Emmett−Teller (BET) isotherm[37] is a widely-used, well-behaved method for extracting effective surface areas and adsorption energies from isotherm data. The method is based on a model of multilayer adsorption which satisfies several conditions: that adsorption occurs on adsorbing sites and on top of adsorbed molecules, that the number of adsorbing sites per layer is constant, that the energy of the first-layer adsorbing sites is uniform, and that molecules in all layers above the first behave as

(57) Lastoskie, C.; Gubbins, K. E.; Quirke, N. *J. Phys. Chem.* **1993**, *7*, 4786.
(58) Machin, W. D. *Langmuir* **1994**, *10*, 1235.

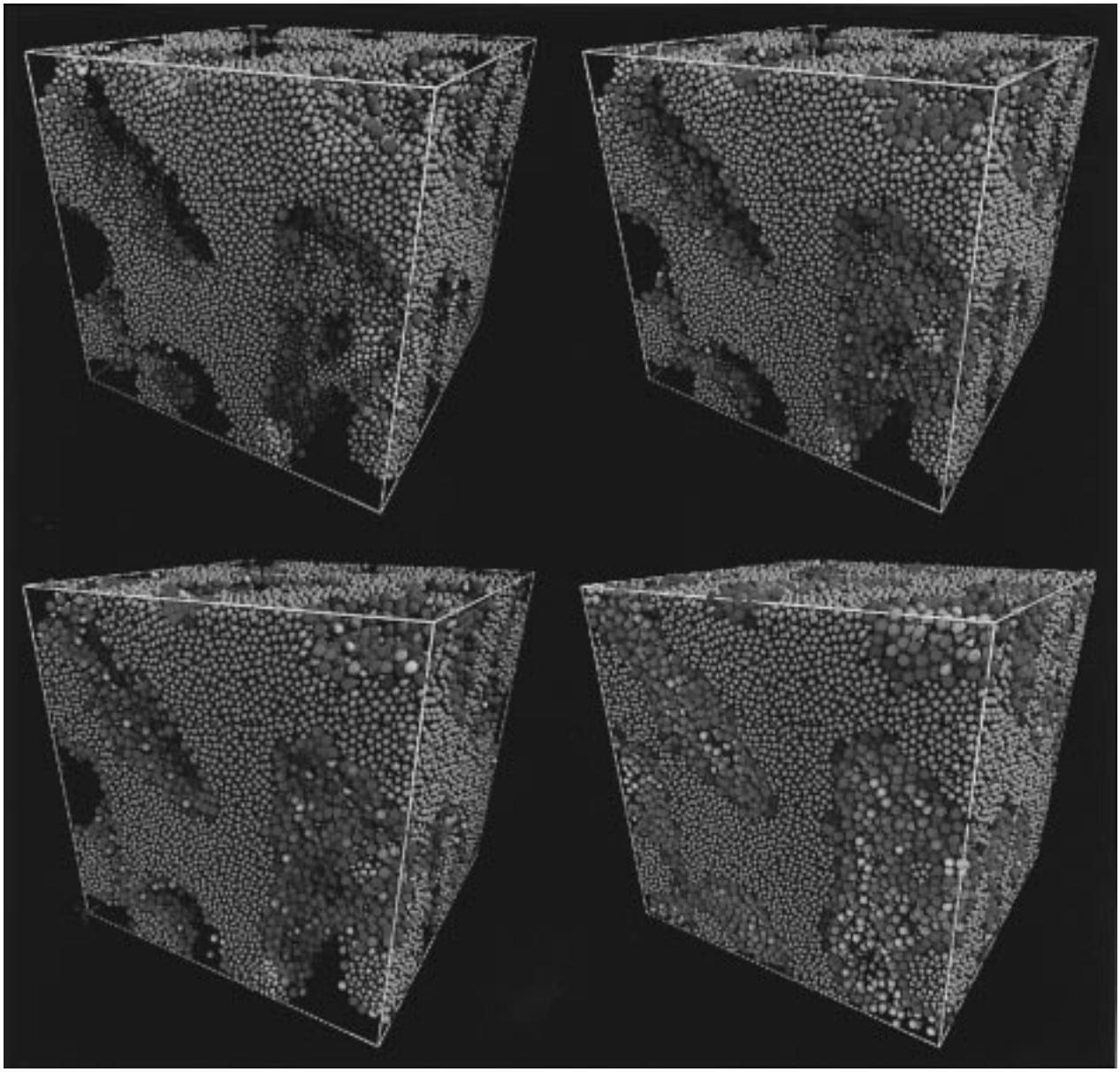

Figure 11. Snapshots of adsorption in the (6c) model CPG system. The configurations are from runs at $P/P^0 = 2.15 \times 10^{-4}$ (upper left), 4.27×10^{-3} (upper right), 1.32×10^{-2} (lower left), and 0.742 (lower right). In these pictures, adsorbate particles are colored according to a potential energy scale, with blue particles having the lowest energy and red particles having the highest.

if in a bulk liquid. Given these conditions, the statistical mechanical problem may be solved by a variety of methods to yield the fundamental equation

$$\frac{P/P^0}{n(1 - P/P^0)} = \frac{1}{n_m c} + \frac{c - 1}{n_m c}(P/P^0) \qquad (2)$$

P/P^0 is the relative pressure, n is the amount adsorbed (per unit mass of adsorbent, say), n_m is the BET *monolayer capacity*, and c is usually related to the net heat of adsorption by $c = \exp(q^{st} - q_L)/RT$, where q^{st} is the isosteric heat of adsorption in the monolayer and q_L is the heat of condensation. Conventionally, adsorption data are plotted as $(P/P^0)/n(1 - P/P^0)$ vs P/P^0, and the n_m and c parameters are determined from the slope and intercept of the resulting line. An excellent discussion of the more subtle aspects of this analysis can be found in Gregg and Sing's book, "Adsorption, Surface Area and Porosity".[59]

(59) Gregg, S. J.; Sing, K. S. W. *Adsorption, Surface Area and Porosity*, 2nd ed.; Academic Press, Inc.: London, 1982.

The monolayer capacity n_m is often divided by some predetermined *monolayer density* to obtain the BET *surface area* of the system. This quantity is often quoted in literature describing porous adsorbents and substrates. The monolayer density is usually taken from adsorption studies of a nonporous material where the surface area can be calculated independently. This procedure implicitly assumes that the average density of the monolayer is transferable between the two materials. If they are chemically similar, this is a reasonable assumption.

In this study we can calculate the surface area of each sample independently, using the stereological methods described above. We can use these to determine the BET monolayer density in each different system and compare them to see how transferable they really are. These data for the glass models and ideal adsorbents are shown in Tables 1 and 2 and discussed below. For all systems, we have fit the BET model only to data with $0.0002 < P/P^0 < 0.25$.

The BET plots for the cylindrical and planar ideal systems are all shown in Figure 13. For all these systems,

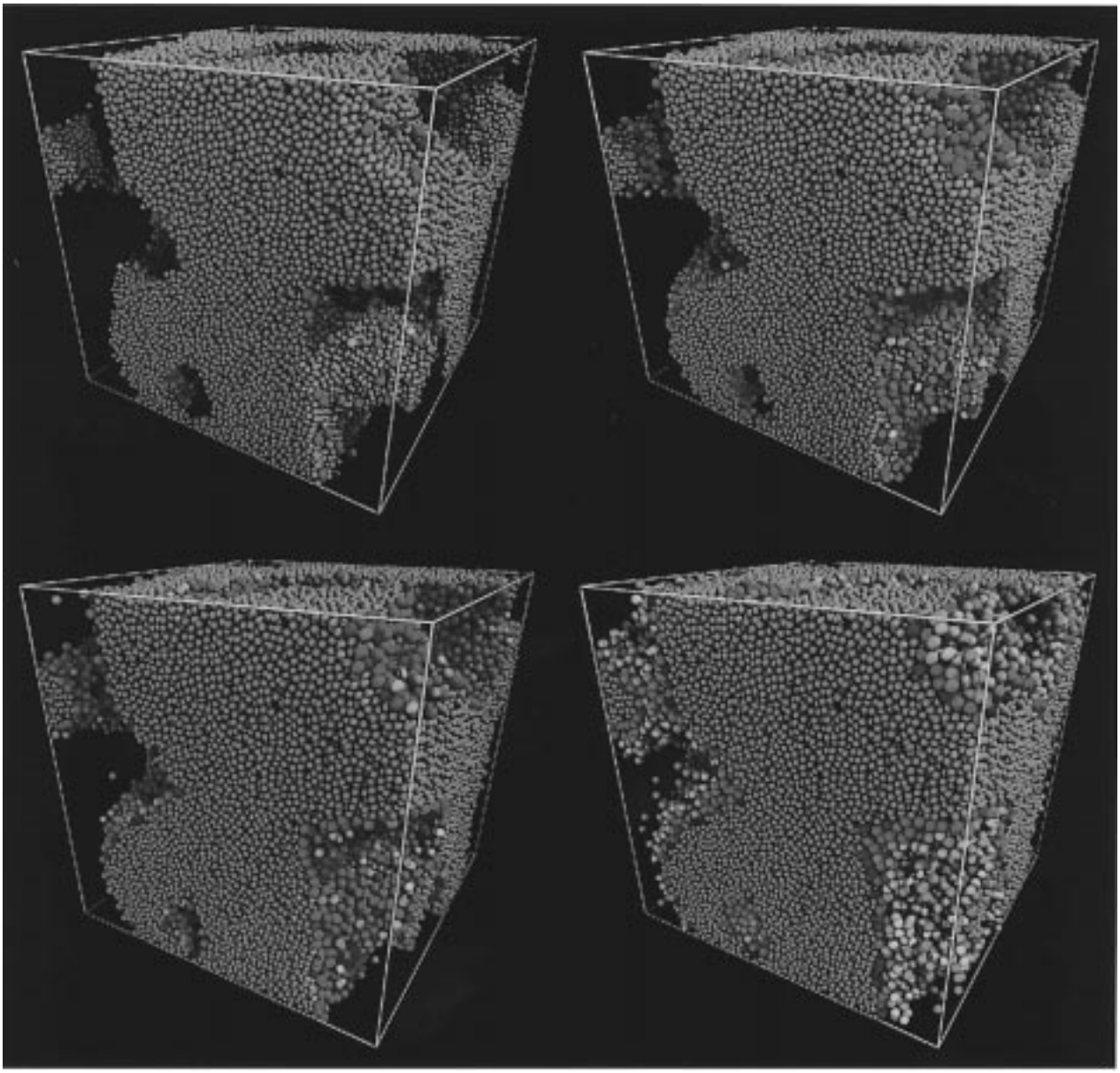

Figure 12. Snapshots of adsorption in the (6d) model CPG system. The configurations are from runs at $P/P^0 = 2.15 \times 10^{-4}$ (upper left), 4.27×10^{-3} (upper right), 1.32×10^{-2} (lower left), and 0.742 (lower right). In these pictures, adsorbate particles are colored according to a potential energy scale, with blue particles having the lowest energy and red particles having the highest.

the method appears to fit the data extremely well. BET plots for the rodlike systems (not shown) are of equally good quality. The corresponding surface density data are shown in Table 2, obtained by dividing the BET monolayer capacity by the surface area determined by geometric methods. As the curvature of the surface is reduced, the monolayer density drops toward its asymptotic planar value of 4.36(5) nm^{-2}. This variation in monolayer capacity correlates well with the average surface energy of these systems (Table 2).

The corresponding BET plots for the networked pore models in the "7" series are shown in Figure 14a. In these systems the fit of the BET equation is also of very high quality, although there is often a very small sigmoid variation in the data. Nevertheless, the BET equation does appear to describe these data very well. The calculated surface densities are shown in Table 1. For the "7" series, these range from a maximum density of 5.38(8) nm^{-2} in the (7a) system to a minimum of 4.49(5) nm^{-2} in the (7d) system, a variation of approximately 20%. The lowest value is significantly higher than the monolayer density of the planar system. As in the ideal systems, the trend in monolayer density correlates well with the trend in average surface energy of these systems. Similar plots for the "6" series and "5" series are shown in parts b and c of Figure 14, respectively. The trends in the data are essentially the same, with different ranges of the monolayer density. For all of the networked systems, the quality of the BET fit to the data improved (measured by linear regression parameters) with increasing pore size.

As mentioned above, the "a" group of materials shows significant microporosity, and the validity of a BET analysis of these isotherms is doubtful. Since the equation does appear to fit well, we present these results along with the others, but this agreement may be an artifact. The very high surface density in these systems is suspect for this reason. However, the trends we find and conclusions that we draw below are not dependent on the smallest pores for support, so this is not a serious problem.

The correlation between surface energy and monolayer density does *not* extend between different groups of systems, and it is not a simple dependence. The monolayer

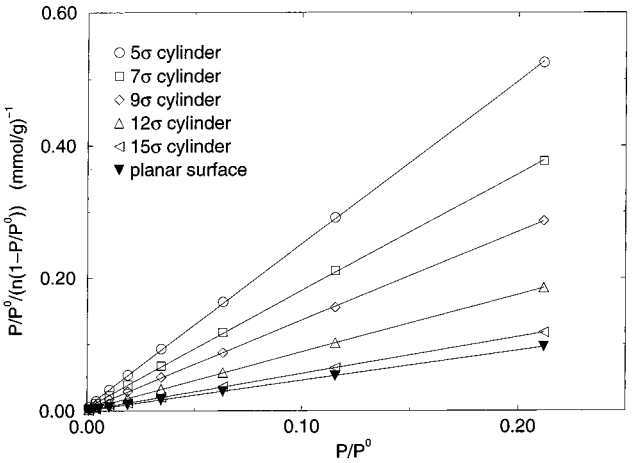

Figure 13. BET analysis plots for all five cylindrical pore systems and the planar pore system. Lines are linear regression fits to the data.

density plotted against the average surface energy for all the different systems is shown in Figure 15. The "ideal" curve is composed of the surface densities for the planar, cylindrical and rodlike systems. While the "7" series and ideal system data seem to fall on the same extended curve, the "5" and "6" series data do not, indicating that the monolayer density in the porous glass systems is a function of more than the average energy. Since the "7" series is in no way distinct, the good agreement between "7" and ideal data is probably coincidental. In general, we expect that as the porosity of the glasses is reduced, the simple cylindrical model will be a better description. This is because the fraction of accessible volume in the system taken up by junctions should decrease, and more of the pore surface will look like a cylinder. As the porosity is increased, we expect to see more voids of complicated geometry and poorer agreement with single pore models. The general correlation between stronger (concave) curvature and increased monolayer density is easily explained. For more strongly curved surfaces, more wall atoms are within a short distance of a point on the surface and the total attractive dispersion energy near the surface is stronger. For convexly curved surfaces the opposite is true, which can be seen in the surface energy data for the rodlike systems (Table 2).

A similar correlation exists between the porosity of the system and its monolayer density. As the porosity is decreased, the average concentration of wall atoms in any given volume is increased, which also leads to an increased attractive potential. However, the *extent* to which this influences adsorption depends on the structure of the material, which itself is dependent on the porosity. Since porous glasses are composed of both concave and convex surfaces, it is hard to predict how strong this effect might be.

Although the monolayer density is correlated with the average pore diameter, this relationship is complex and there is no quantitative agreement between any pair of systems. These data appear in Figure 16 and show that although the same general trend is present for each family of pores, there is no quantitative agreement between the ideal cylinders and any of the porous glass systems. The different curves appear to be offset by different amounts relative to the ideal system and to also have different curvatures. Specifically, the monolayer density in the networked systems is much more strongly dependent on the pore size than it is in the ideal systems. This may reflect the different porosities in these systems. Since

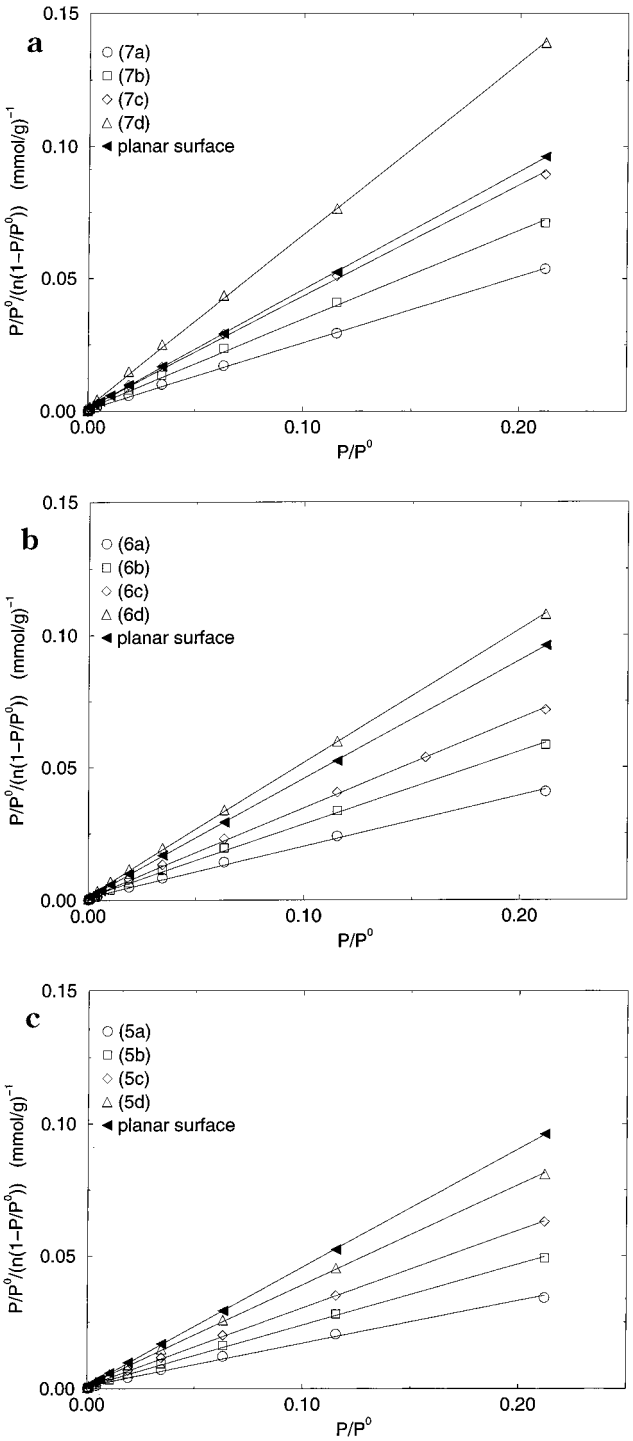

Figure 14. BET analysis plots for the four CPG models in the "7" series (a), in the "6" series (b), and the "5" series (c). The planar surface system is included in each plot for comparison. Lines are linear regression fits to the data.

increasing the porosity seems to decrease the surface density in the porous glasses, the offset in the different curves correlates well with the porosity.

We should not expect quantitative agreement between the monolayer densities of a networked sample and a single cylinder with the same average diameters. Since the networked sample contains larger and smaller sections of pore, it is often modeled as a collection of cylinders of different diameter. The average monolayer density would therefore be a weighted average over the monolayer densities of these cylinders. The presence of constrictions would lead to an increase in average monolayer density,

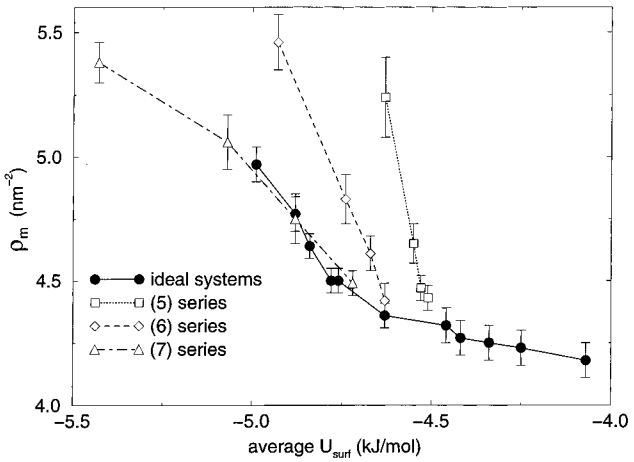

Figure 15. Monolayer density (ρ_m) vs average surface energy, for all systems. Numerical data are in Tables 1 and 2. The ideal system data are the full set of cylinders, rods, and the planar surface, put together.

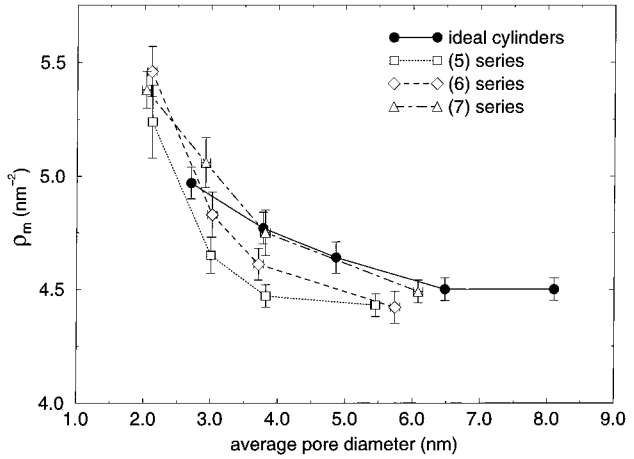

Figure 16. Monolayer density (ρ_m) vs average pore diameter, for all CPG systems and ideal cylinders. Numerical data are in Tables 1 and 2.

and the presence of larger voids would lead to a decrease. Since these variations in monolayer density decay quickly as the pores become larger and the experimental pore size distribution appears to be very roughly symmetric,[6] we might expect to see a net *increase* in the monolayer density of the networked system due to polydispersity of pore size. This increase is cancelled in part by the larger surface area in the large pores, which skew the average in the other direction. In Figure 16 some of the CPG points fall below the ideal system curve and some fall above, indicating a net increase for small pores, and a decrease for large pores. This increase for small pores may be due to microporosity in the samples and should not be relied upon.

6. Discussion

Analysis of the BET monolayer densities for the model glasses indicates that neither the average surface energy nor the average pore diameter of the porous glass materials can be quantitatively related to that of the ideal cylinder systems via adsorption data analysis. That is, ideal systems and model CPG systems with the same surface energies do *not* have the same monolayer densities, and ideal systems and model CPG systems with the same average radius also do *not* have the same monolayer densities. This occurs because these systems have substantial regions with convex curvature and noncylindrical shape.

This leads to the conclusion that it may not be appropriate to describe these porous materials as collections of straight cylinders. The relationship between surface energetics, pore diameter, and monolayer density appears to be different for the porous glasses and the ideal cylinders. Attempting to describe the adsorption isotherm of the porous glasses by using a collection of cylinders would likely *overestimate* the average pore size, since the monolayer capacity of a model pore material is systematically lower than that of an ideal cylinder of similar diameter (Figure 16), for diameters greater than about 4 nm. Likewise, an attempt to fit a porous glass' surface energy distribution might *underestimate* the average surface energy, since for a given monolayer capacity the corresponding average surface energy is systematically greater (less attractive) in the model glasses than in the ideal cylinders (Figure 15).

These systematic errors are likely to be small, except in systems with very small pores. In no case do the data we have presented vary (between ideal and CPG systems) by more than about 20%, and they are frequently (especially for the "7" series of glasses) much closer than that to the ideal system data.

The monolayer densities we report indicate that the common practice of dividing the BET monolayer capacity by a reference value for the surface density (usually taken as one molecule per 16.2 Å^2, for nitrogen) leads to a systematic overestimation of the surface area in small pores; the smaller the pore, the larger the overestimation. However, if we use this procedure with the monolayer density taken from the ideal planar system (the appropriate reference surface for the model glasses), this error is less than 25% for all of the networked systems that we have studied and less than 10% for the larger systems. Since these glasses represent the extreme small-pore end of CPG materials, we expect that for most experimental systems this procedure gives a quite accurate surface area.

Despite these systematic quantitative differences between systems, the BET equation appears to fit all of our data very well, at least for the first two monolayers' thickness. (At higher pressure, the BET model performs poorly because the vapor begins to condense, following type IV behavior; only at low pressures is this model applicable to both type II and type IV isotherms.) This is remarkable because the systems we have studied do not satisfy *any* of the requirements of the BET model! We point out that the average pore size in these calculations is always at least 5.5 times the diameter of the adsorbate, so that we are not inadvertently applying this model to wholly microporous materials. For all but the "a" group of systems, the average pore diameter is much larger than this.

Furthermore, it is only the smaller-pore systems that we have studied that show appreciable systematic deviations from the ideal geometry behavior. For most porous glasses, which can have pore diameters as large as 400 nm, these errors will be much smaller than other difficulties commonly encountered in isotherm analysis. The BET analysis should give an excellent estimate of the monolayer capacity in these systems; any systematic error in the resulting surface areas will be due to chemical differences between the reference surface and surface of interest.

These general conclusions do not depend on the exact details of the models or procedures that we have used and should be generally valid for this class of materials. If we have overestimated or underestimated any of the Lennard-

Jones potential parameters, it would affect all the monolayer densities in a systematic (and relatively small) way and the qualitative relationships between different data would not change.

The principal weakness of these models (in terms of direct comparison with experimental systems) is that the surface molecular structure is not correct; the faceting behavior of the amorphous Lennard-Jones solid does not closely resemble the structures found on surfaces of amorphous silica. Also, this model ignores any surface functionality, though this is probably not a large effect when comparing with nonderivatized silica. Lastly, we have omitted the relatively weak interaction between the nitrogen quadrupole and the electrostatics of the glass. Nevertheless, these model materials seem to belong to the same general class of structures as controlled-pore glasses, so that we can use them to good effect for studying characterization methods and larger-scale structural properties. The only effect of the different surface structure is to modify the monolayer density in a systematic way, so that data from simulation will be slightly shifted relative to experiment. This offset might be controlled by fitting the potential parameters to adsorption data rather than gas-phase data for the component species; this will be the subject of a future study.

Because of the complexity of these pore structures, it is difficult to show conclusively that these materials *are* in the same general class as experimentally prepared porous glasses, although the evidence does suggest that this is true. The porosities and surface areas are directly comparable between these model materials and controlled-pore glasses, and the chord length distributions have the same general shape. Also, planar sections of these model materials appear quite similar to electron micrographs of real porous glasses.[2,3] Although it is possible for us to measure more topologically complex parameters such as the *connection number*[42] of the pore network, there is no experimental measurement of this quantity with which to compare.

In this study we have developed a procedure for generating model porous materials with the same general properties as controlled-pore glasses. We have made a series of these materials with different average pore sizes and porosities and studied these structures using geometric methods. We have obtained adsorption isotherms for these materials and analyzed these data using standard techniques. We find that the method of BET isotherm analysis consistently overestimates the surface area in glasses with very small pores because the monolayer density is dependent on the average pore diameter in these glasses. Furthermore, the networked systems can exhibit qualitatively different trends in these data than do single cylinders, which indicates that it may be inappropriate to model the networks as collections of unconnected cylinders. All of these results are significant only for the small-pore end of this family of materials; our data indicate that for materials with average pore diameters much larger than 6 nm, the local curvature of the surface only negligibly affects the structure of the monolayer and the BET method can accurately predict the surface area of the glass.

Acknowledgment. We thank the National Science Foundation (Grant No. CTS-9508680) for their support of this work and for a Metacenter Grant (No. MCA93S011P) which made these calculations possible and the staff of the Cornell Theory Center for their general assistance. L.D.G. thanks the National Science Foundation for a CISE Fellowship.

LA9710379